1982) but again this method is not practicable for general spectroscopic use since the signal-to-noise ratio would be very poor. The third method which seeks to control the Bragg width by oblique Bragg reflections has been widely used (Renninger, 1961, 1967; Kikuta & Kohra, 1970; Kikuta, 1971; Matsushita, Kikuta & Kohra, 1971; Hashizumi & Kohra, 1971; Bonse & Graeff, 1973; Kohra, 1972). Kohra & Kikuta (1968) summarize fairly completely the relevant literature so that not all references need be mentioned here. In essence, cutting the surface of a crystal at angle α to the Bragg planes reduces the range of Bragg reflection by a factor $b^{1/2}$, where $b = \sin(\theta - \alpha)/\sin(\theta - \alpha)$. Oblique incidence at $\frac{1}{2}°$ to the surface yields a narrowing factor of ten at a Bragg angle $\theta = 60°$ but such small glancing angles are difficult to achieve, result in specular external reflection and, by definition, do not permit the tuneability necessary for spectroscopy. However, it would appear to be possible to achieve large narrowing factors by combining this method and the present one. For example, Kikuta (1971) achieved $b = 573$ and we demonstrate herein a further factor of four so that the total narrowing in a combined device could be $4b^{1/2} = 100$ with the 422 reflection from silicon. Since the energy resolution of a single-crystal Bragg spectrometer based on the 422 Bragg reflection is $1{\cdot}4 \times 10^{-6}$ (Beaumont & Hart, 1974), the energy resolution of an oblique-offset multiple-reflection Bragg spectrometer would then be $1{\cdot}4 \times 10^{-8}$; quite adequate for many experiments which have been proposed using synchrotron radiation sources, for example, the measurement of inelastic X-ray scattering due to phonons. The construction has the added advantage that setting up could be done in the low-resolution mode with high intensity and the resolution would be varied to suit the problem in hand.

References

AUTHIER, A. (1961). *Bull. Soc. Fr. Minéral. Cristallogr.* **84**, 51–89.
BEAUMONT, J. H. & HART, M. (1974). *J. Phys. E*, **7**, 823–829.
BOLLMAN, V. L., BAILEY, H. H. & DUMOND, J. W. M. (1938). *Phys. Rev.* **54**, 792–801.
BONSE, U. & GRAEFF, W. (1973). *Z. Naturforsch. Teil A*, **28**, 558–564.
BONSE, U. & HART, M. (1965). *Appl. Phys. Lett.* **7**, 238–240.
COLE, H., CHAMBERS, F. W. & WOOD, C. G. (1961). *J. Appl. Phys.* **32**, 1942–1945.
CUSATIS, C., HART, M. & SIDDONS, D. P. (1982). *Acta Cryst.* A**39**, 199–202.
DUMOND, J. W. M. (1937). *Phys. Rev.* **52**, 872–883.
HART, M. & RODRIGUES, A. R. D. (1978). *J. Appl. Cryst.* **11**, 248–253.
HART, M. & RODRIGUES, A. R. D. (1979). *Philos. Mag.* B**40**, 149–157.
HASHIZUMI, H. & KOHRA, K. (1971). *J. Phys. Soc. Jpn*, **31**, 204–216.
JAMES, R. W. (1948). *The Optical Principles of the Diffraction of X-rays*. London: Bell.
KIKUTA, S. (1971). *J. Phys. Soc. Jpn*, **30**, 222–227.
KIKUTA, S. & KOHRA, K. (1970). *J. Phys. Soc. Jpn*, **29**, 1322–1328.
KOHRA, K. (1972). *Proc. VIth International Conference on X-ray Optics and Microanalysis*, pp. 35–43. Univ. of Tokyo Press.
KOHRA, K. & KIKUTA, S. (1968). *Acta Cryst.* A**24**, 200–205.
MATSUSHITA, T., KIKUTA, S. & KOHRA, K. (1971). *J. Phys. Soc. Jpn*, **30**, 1136–1144.
OKKERSE, B. (1963). *Philips Res Rep.* **18**, 413–431.
RENNINGER, M. (1961). *Z Naturforsch. Teil A*, **16**, 1110–1111.
RENNINGER, M. (1967). *Adv. X-ray Anal.* **10**, 32–39.
RODRIGUES, A. R. D. & SIDDONS, D. P. (1979). *J. Phys. E*, **12**, 403–408.

Acta Cryst. (1984). A**40**, 507–514

Propagation of X-ray Beams in Distorted Crystals (Bragg Case). I. The Case of Weak Deformations

BY J. GRONKOWSKI* AND C. MALGRANGE

Laboratoire de Minéralogie–Cristallographie, Universités Pierre et Marie Curie (Paris VI) et Paris VII, Tour 16, 4 *place Jussieu*, 75230 *Paris CEDEX* 05, *France*

(*Received* 1 *August* 1983; *accepted* 12 *March* 1984)

Abstract

It has been commonly admitted that the theories of X-ray propagation in distorted crystals based on the principles of geometrical optics [Penning & Polder (1961). *Philips Res. Rep.* **16**, 419–440; Kato (1963). *J. Phys. Soc. Jpn*, **18**, 1785–1791; Kato (1964). *J. Phys. Soc. Jpn*, **19**, 67–71, 971–985] were applicable only in the transmission (Laue) case. It is demonstrated in this paper that they can be applied more generally in all cases where beams can be defined, *i.e.* also in the Bragg case outside the total reflection range. Simple formulae for the case of a constant strain gradient in symmetric Bragg geometry are derived from a general formulation of the basic equation of geometrical theory using a new universal parameter a. They are verified by solving Takagi's

* Present and permanent address: Institute of Experimental Physics, Warsaw University, 00-681 Warsaw, Hoża Street 69, Poland.

0108-7673/84/050507-08$01.50

equations numerically. The results are visualized by means of an original method of ray tracing directly from Takagi's equations.

1. Introduction

The propagation of X-rays in deformed crystals has been the subject of many theoretical and experimental studies since 1961 when Penning & Polder first published their theory of geometrical optics of wavefields based on an analogy with the propagation of light in inhomogeneous media. Wave-optical considerations developed later by Kato (1963, 1964), Kambe (1965, 1968) and Chukhovskii & Shtolberg (1970) provided a more rigorous foundation for Penning & Polder's theory and showed that its basic equation could also be derived from an Eikonal approach. All these theories assumed that the wave vectors of wavefields propagating in the crystal were real and they were generally supposed to be valid only in the transmission (Laue) case. Detailed reviews of geometrical optics theories can be found in articles by Malgrange (1975) and Hart (1980); the latter also contains a survey of experimental works and a bibliography of the subject.

In 1964, Bonse published his geometrical theory (Bonse, 1964*a*), based on a variational principle, which allowed for wavefields with wave vectors having large imaginary parts. Therefore, it was supposed to be fully applicable in the reflection (Bragg) case, including incidence angles lying within the total reflection range. On the other hand, it could be regarded as a generalization of Penning–Polder theory, especially since for wavefields with real wave vectors (in the Bragg case those excited outside the total reflection range) its basic equation reduced to that of other geometrical theories (Bonse, 1964*a*).

However, as was soon demonstrated by Penning (1966) (and recently confirmed by Chukhovskii, 1981), it is not possible to describe wavefields with complex wave vectors in terms of classical ray concepts of geometrical optics. Nevertheless, Bonse's theory provided a valid description of the propagation of wavefields with real wave vectors which are generated in the Bragg case outside the total reflection range (in the flanks of the rocking curve). Therefore, it could be successfully applied for calculations of beam trajectories in a bent crystal (Bonse, 1964*b*; Bonse & Graeff, 1973) or a crystal with a dislocation line (Bonse, 1964*c*), demonstrating the effect of deflection of X-rays to the crystal surface.

On the other hand, all the other theories of geometrical optics were used exclusively to interpret the results of experiments performed in the Laue case. As a consequence of this 'division of application field' a view has developed throughout the literature that the range of applicability of Penning–Polder theory was limited to the Laue case.*

The aim of the present work is to show that Penning–Polder theory can be used without any difficulty to describe X-ray propagation in slightly distorted crystals not only in the transmission case but in the Bragg case as well, provided that the incident angle is chosen outside the total or the 'quasitotal' (for absorbing cases) reflection range. We shall develop the basic equations of the theory for ray paths and intensities in the Bragg case and compare the so-obtained trajectories with the corresponding numerical solutions of Takagi's equations (Takagi, 1969), using as a helpful tool an original method of ray tracing (§ 3). The demonstrated general applicability of Penning–Polder theory will be exploited in the following paper (Gronkowski & Malgrange, 1984) dealing with the case of strong distortion and the phenomenon of new wavefield creation.

2. Geometrical optics

(*a*) *Conditions of applicability*

Geometrical optics can only be used when beams can be introduced. Let us consider, for example, a plane wave limited by a slit of width equal to e. In the air the width of the beam given by the slit is constant as long as the path length is smaller than e^2/λ (where λ is the wavelength) and only Fresnel diffraction phenomena may appear on the edges of the beam. Beyond this path length the beam diverges with an angle λ/e because of diffraction (Fraunhofer diffraction). Such diffraction phenomena have been studied by Authier & Malgrange (1966) in the case of X-ray diffraction in perfect crystals where the divergence of the beam is amplified by a factor of the order of $\Lambda \sin\theta_B/\lambda$ for the exact Bragg incidence (where Λ is the extinction length) which decreases rapidly with the departure from the Bragg angle. Consequently, the path length beyond which the beam diverges is of the order of $e^2/\Lambda \sin\theta_B$ for Bragg incidence and increases with the departure from the Bragg angle.

A generalization of the calculations due to Authier & Malgrange (1966) to the case of distorted crystals is not straightforward. However, some of their qualitative conclusions can be readily extended to distorted crystals, providing an explanation of the broadening of the beam visible in some cases (*cf.* Figs. 6*a*, *b*, *c*). This phenomenon will be the subject of a separate paper.

* Perhaps the only exception is a short remark which can be found in the review article by Hart (1980, p. 250): 'Agreement with theory, both in the Laue case and in the flanks of the Bragg-case rocking curve (when the same ray paths are generated), indicates very clearly the value of concentrating upon the details of wavefield propagation rather than upon the detailed diffraction geometry, which is relatively unimportant.'

(b) *Basic equations*

The basic equation of geometrical optics of X-rays can be written most generally in the form given by Penning & Polder (1961)

$$\mathrm{d}(1/\xi - \xi) = 2\beta \, \mathrm{d}x, \tag{1}$$

where x is the coordinate along the reflecting planes, β is the strain gradient defined by the formula

$$\beta = \frac{1}{kC(\chi_h \chi_{\bar{h}})^{1/2} \cos\theta_B} \frac{\partial^2(\mathbf{h} \cdot \mathbf{u})}{\partial s_0 \, \partial s_h} \tag{2}$$

with $k = 1/\lambda$ the wave vector of the radiation, C the polarization constant, θ_B the Bragg angle, χ_h and $\chi_{\bar{h}}$ the Fourier coefficients of the dielectric susceptibility χ, $\mathbf{u}$ the displacement vector, $\mathbf{h}$ the diffraction vector, s_h and s_0 the coordinates along the reflected and refracted directions, respectively.

Note that here the definition for β due to Kato (1964) is used; it differs from that of Penning & Polder only by the sign.

ξ is defined as the ratio of the amplitudes D_h and D_0 of the reflected and refracted waves, respectively,

$$\xi = D_h / D_0. \tag{3}$$

The ξ parameter (Fig. 1) determines the position of the tie point on the dispersion surface and consequently the physical characteristics of the corresponding wavefields: its type (1 or 2) since ξ is negative for wavefield 1 and positive for wavefield 2, and its direction of propagation. ξ is in general complex either due to absorption and then its imaginary part is small or due to 'extinction', meaning here the strong damping phenomenon appearing in the crystal in the total reflection range in the Bragg case.

Equation (1) and the quasi-classical description of wavefield propagation in terms of geometrical optics is valid only for wavefields with almost real ξ values.*

* A practical estimate of the maximum allowable value for the ratio of the imaginary part to the real part of ξ was found to be 0·1.

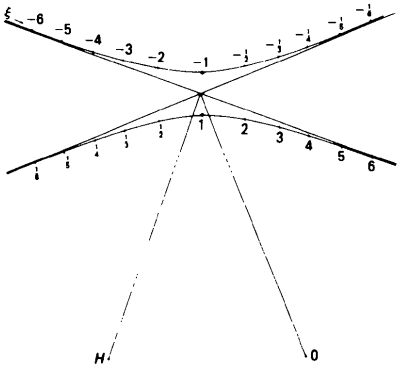

Fig. 1. Variation of ξ as a function of tie-point position on the dispersion surface (after Penning & Polder, 1961). $\xi < 0$ for wavefield (1), $\xi > 0$ for wavefield (2).

For wavefields with large imaginary parts of ξ which are excited only in the total reflection range or very close to it in the Bragg case, it is not possible to construct a ray theory as shown by Penning (1966). Therefore, (1) describes well the propagation of wavefields which are generated in the crystal in the Laue case and outside the total reflection range in the Bragg case. It should be stressed that it is not important how a wavefield with an almost real given value of ξ has been generated in the Laue case or Bragg case, symmetric or asymmetric reflection. Once it exists in the crystal it propagates according to (1) which gives the variation of ξ, that is the variation of the tie-point position, along the dispersion surface.

Let us introduce a new parameter a (Malgrange, 1975),

$$a = \tfrac{1}{2}(1/\xi - \xi). \tag{4}$$

Then (1) assumes a particularly simple form

$$\mathrm{d}a = \beta \, \mathrm{d}x. \tag{5}$$

The parameter a has a very simple geometric representation. Let us consider a given point P on the dispersion surface (Fig. 2a) and draw through it a straight line parallel to the reflecting planes and intersecting the dispersion surface in the vacuum (T_0') in Q. Then it can be shown very easily that

$$\overline{LQ} = \frac{C(\chi_h \chi_{\bar{h}})^{1/2}}{\lambda \sin 2\theta_B} a = a/2\Lambda \sin\theta_B, \tag{6}$$

where

$$\Lambda = \lambda \cos\theta_B / C(\chi_h \chi_{\bar{h}})^{1/2}. \tag{7}$$

Equation (5) gives the variation of Q along T_0' and consequently the variation of the tie-point position on the dispersion surface once the initial point is given. The initial position of the tie point is determined by the incidence conditions. It is described by a_i, the initial value of a at the entrance surface:

$$a_i = \tfrac{1}{2}(1/\xi_i - \xi_i) \tag{8}$$

and

$$\xi_i = (\gamma_0/|\gamma_h|)^{1/2}(|C|/C)(\chi_h \chi_{\bar{h}})^{1/2}/\chi_{\bar{h}} \times \{\eta_i \pm [\eta_i^2 + S(\gamma_h)]^{1/2}\} S(\gamma_h), \tag{9}$$

where $S(\gamma_h)$ is equal to 1 if $\gamma_h > 0$ (Laue case) and -1 if $\gamma_h < 0$ (Bragg case) and η_i is the initial value of the parameter η:

$$\eta_i = (\gamma_0/|\gamma_h|)^{1/2}/|C|(\chi_h \chi_{\bar{h}})^{1/2} \times [\Delta\theta \sin 2\theta_B - (\chi_0/2)(\gamma_h/\gamma_0 - 1)], \tag{10}$$

$\Delta\theta = \theta - \theta_B$ is the deviation from the Bragg angle, γ_0 and γ_h are the direction cosines of the incident and reflected beams respectively, χ_0, χ_h, $\chi_{\bar{h}}$ are respectively the 0, h and $-h$ Fourier coefficients of χ. In the special

case of a constant strain gradient β, the general equation (5) becomes

$$a(x) = a_i + \beta x. \tag{11}$$

The beam trajectories are sections of hyperbolae given by the equation (Malgrange, 1975)

$$[\beta z/\tan\theta_B \mp (1+a_i^2)^{1/2}]^2 - (\beta x + a_i)^2 = 1. \tag{12}$$

In (9) and (12) the upper (lower) sign corresponds to wavefield 1 (2). In the transmission (Laue) case, an incident beam with a departure $\Delta\theta$ from the Bragg angle excites on the dispersion surface in vacuum (T_0') a point M and induces in the crystal two wavefields of different types (1, 2) with respective tie points P_1 and P_2 (Fig. 2*a*). The lines drawn parallel to the reflecting planes from P_1 and P_2 cut T_0' at Q_1 and Q_2 and one deduces from (6) that

$$a_{i1} = \overline{LQ_1}(2\Lambda \sin\theta_B),\ a_{i2} = \overline{LQ_2}(2\Lambda \sin\theta_B), \tag{13}$$

a_{i1} and a_{i2} can also be calculated from (8) and (9). The beam paths in the crystal are hyperbolae given by (12). The associated tie points move from P_1 and P_2 to P_1' and P_2', respectively. They are related to Q_1' and Q_2' determined from $\overline{Q_1Q_1'} = \overline{Q_2Q_2'}$.

In the reflection (Bragg) case an incident beam with a departure from Bragg angle $\Delta\theta$ *outside* the total reflection range induces two tie points P_{iA} and P_{iB} on the same branch of the dispersion surface (Fig. 2*b*) depending on the sign of η_i. Only one of the two excited wavefields is directed towards the inside of the crystal (here P_{1A} or P_{2B}). In geometrical optics where narrow beams are considered the other wavefield has only to be taken into account if the beam is reflected at the exit surface.

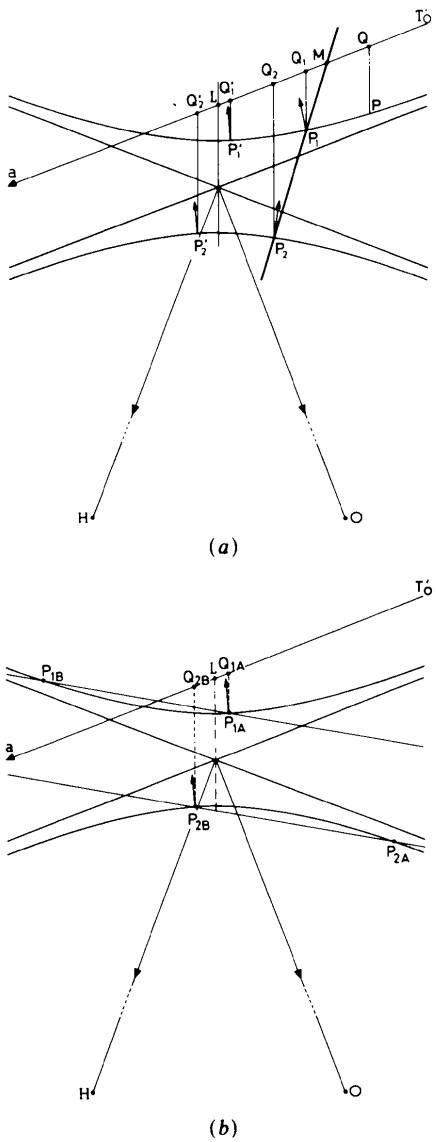

Fig. 2. Geometrical interpretation of the parameter a, where $a(P) = \overline{LQ}/(2\Lambda \sin\theta_B)$. (*a*) Laue case, (*b*) Bragg case.

(*c*) *The symmetric Bragg case*

Let us now describe in detail the application of geometrical optics for the especially simple case of Bragg diffraction in a thick centrosymmetric crystal deformed with a constant strain gradient β, assuming for simplicity $C = 1$ and zero absorption.

Formulae (9) and (10) become

$$\xi_i = \eta_i - S(\eta_i)(\eta_i^2 - 1)^{1/2} \tag{14}$$

$$\eta_i = (\Delta\theta \sin 2\theta_B + \chi_0)/|\chi_h|, \tag{15}$$

where $S(\eta_i) = 1$ if $\eta_i > 0$ and $S(\eta_i) = -1$ if $\eta_i < 0$. As the incidence angle deviation $\Delta\theta$ lies outside the total reflection region, we always have $|\eta_i| > 1$. If we substitute (14) in (8) we obtain the formula for the initial value of a_i as a function of η_i:

$$a_i = S(\eta_i)(\eta_i^2 - 1)^{1/2}. \tag{16}$$

(Note that in the symmetric Laue case we would have simply $a_i = \eta_i$.) Equation (12) for the trajectory becomes

$$\left(\frac{\beta z}{\tan\theta_B} + \eta_i\right)^2 - [\beta x + S(\eta_i)(\eta_i^2 - 1)^{1/2}]^2 = 1. \tag{17}$$

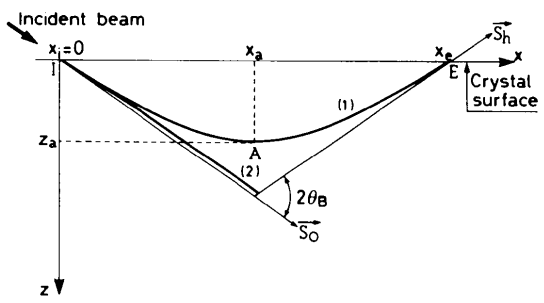

Fig. 3. Beam trajectories in the symmetric Bragg case: (1) $\eta_i\beta < 0$, (2) $\eta_i\beta > 0$.

The beam path is deflected to the inside of the crystal if $\eta_i\beta > 0$ and to the crystal surface if η_i and β are of opposite signs (Fig. 3). In the latter case the coordinates of the apex of the hyperbolic trajectory are given by

$$x_a = -S(\eta_i)(\eta_i^2 - 1)^{1/2}/\beta \tag{18}$$

$$z_a = -(\tan\theta_B/\beta)[\eta_i - S(\eta_i)]. \tag{19}$$

Note that in the symmetric case the apex A of the hyperbola is always reached in the middle part of the trajectory so that

$$x_e = 2x_a, \tag{20}$$

where x_e is the coordinate of the beam exit point (the 'range' of the deflected beam). Furthermore, using (4), (5), (19) and (20) one easily obtains

$$\xi_e = 1/\xi_i, \tag{21}$$

where ξ_e is the value of ξ at the beam exit point.

(*d*) *Intensities in the Bragg case*

In the Bragg case the incident beam of intensity I_0 is partly reflected at the entrance surface with an intensity I_{ha} (Fig. 4). The rest of the intensity I_i goes into the only wavefield which propagates in the crystal. Using boundary conditions and the principle of conservation of energy one gets:

$$\frac{I_i}{I_0} = 1 - \frac{|\xi_i|^2}{|\gamma|}, \qquad \frac{I_{ha}}{I_0} = \frac{|\xi_i|^2}{|\gamma|}, \tag{22}$$

ξ_i is the value of the parameter ξ at the entrance surface and γ the ratio γ_0/γ_h.

If there is no absorption the intensity is conserved along the beam. If the absorption is not negligible the intensity at the exit of the beam I_e is given by (Malgrange, 1975)

$$\frac{I_e}{I_i} = \exp\left(-(\mu_0 x/\cos\theta_B)\left\{1 \mp (1/\beta x)|\chi_{ih}/\chi_{i0}| \times \log\left[\frac{a_e + (1+a_e^2)^{1/2}}{a_i + (1+a_i^2)^{1/2}}\right]\right\}\right) \tag{23}$$

or equivalently

$$\frac{I_e}{I_i} = \exp\{-(\mu_0 x/\cos\theta_B) \times [1 - (1/\beta x)|\chi_{ih}/\chi_{i0}| \log \xi_e/\xi_i]\}, \tag{24}$$

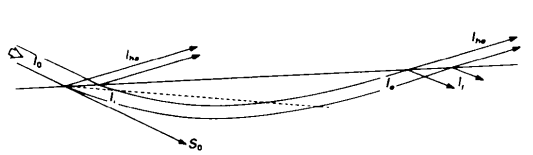

Fig. 4. Beams issuing from an incident beam of intensity I_0 in the Bragg case.

where μ_0 is the linear absorption coefficient, a_e and ξ_e are the respective values of a and ξ at the beam exit point. There, the intensity is split among the reflected beam in the air of intensity I_{he} and a wavefield of intensity I_j reflected inside the crystal. Using boundary conditions and the energy conservation principle one gets:

$$\frac{I_{he}}{I_e} = 1 - \frac{|\gamma|}{|\xi_e|^2}, \qquad \frac{I_j}{I_e} = \frac{|\gamma|}{|\xi_e|^2}. \tag{25}$$

In the special case of symmetric reflection and zero absorption (21), (22), (24) and (25) give

$$\frac{I_{ha}}{I_0} = |\xi_i|^2, \qquad \frac{I_{he}}{I_0} = (1 - |\xi_i|^2)^2,$$

$$\frac{I_j}{I_0} = (1 - |\xi_i|^2)|\xi_i|^2 = |\xi_i|^2 \frac{I_i}{I_0}.$$

The wavefield reflected at the beam exit towards the inside of the crystal propagates along a hyperbolic trajectory as the initial wavefield. It is reflected for the second time at the crystal surface and so on, in an analogous manner to a wave in a wave guide but its intensity decreases rapidly ($|\xi_i|$ is less than 1), the more rapidly the greater $|\eta_i|$.

3. Numerical techniques used in the computer experiment

The X-ray diffraction in the Bragg case for a thick crystal distorted by a constant strain gradient β was treated rigorously by Chukhovskii, Gabrielyan & Petrashen' (1978) who formulated the solution in the integral form of the Huyghens–Fresnel principle and obtained the exact Green–Riemann functions suitable for a general analysis of the problem. They demonstrated that the solutions for one type of wavefield was of a 'waveguide' nature; energy was transported in a channel parallel to the surface, undergoing successive reflections from both walls of the channel. The description in terms of geometrical optics given in § 2 (Fig. 4) is in good agreement with these results. As the intensity of the beam which is internally reflected at the point E (Fig. 3) of the surface (upper wall of the channel) does not exceed 7% of the incident intensity in the symmetric Bragg case if $|\eta_i| > 2$ [*cf.* (25)], practically it is sufficient to deal only with a single trajectory (*IAE* in Fig. 3).

(*a*) *Numerical integration of Takagi's equations*

Since the mathematical form of the rigorous solution of Chukhovskii, Gabrielyan & Petrashen' (1978) is rather complicated, in the present work we choose to solve Takagi's equations numerically using the method of half-step derivative due to Authier, Malgrange & Tournarie (1968). The algorithm is described in detail in the above reference; in the Bragg

case it was applied for the first time by Bedynska (1973) who calculated the intensity distribution of the diffracted beam for a thick crystal with a screw dislocation normal to the surface, using the following plane-wave boundary conditions (Fig. 5): (1) $D=1$ on AB; (2) D_0 and D_h according to dynamical theory for perfect crystals along AS.

The calculations were made line by line parallel to the s_0 axis. As the incident wave was assumed to be plane and the distortion field in that case was considerable only in the immediate vicinity of the dislocation line, such a choice of boundary conditions was perfectly justified. In the present calculations, however, we cannot assume an incident plane wave; the beam suitable for geometrical optics studies has to be limited in size (but not too narrow if effects due to diffraction in the optical sense are to be minimized). We found it a good compromise to perform the calculations using a beam with a Gaussian distribution of the incident amplitude D along the crystal surface:

$$D(x)=\exp\{-4x^2/\sigma^2\},$$

since a Gaussian wave packet does not change shape appreciably in the crystal (Penning, 1966). On the other hand, it represents quite well the physical reality of incident beams which can be obtained in the experimental practice (Bonse & Graeff, 1973) and it falls off very quickly away from the maximum (D is of the order of 10^{-7} for $|x|=2\sigma$). Thus, we can put simply $D_0=D_h=0$ as the boundary conditions along the s_0 characteristics (AS) if the starting point A of the integration network is chosen sufficiently far away from the point of incidence I of the center of the beam. Then the parasitic transient solutions which appear initially due to this choice of boundary conditions practically do not influence the values of D_0 and D_h in the important part of the integration network and the correct values are established quickly. We found that it was sufficient to choose the starting point A at a distance of 2σ from the incident point I of the center of the beam to reduce any

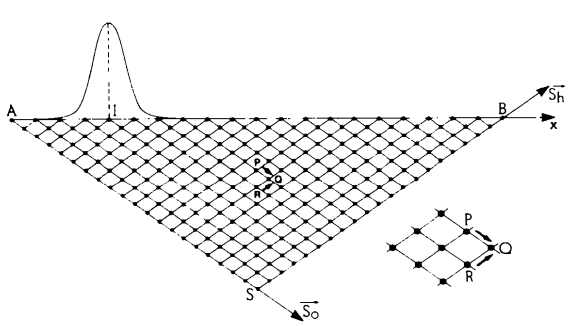

Fig. 5. The integration network in the Bragg case (after Bedynska, 1973). The Gaussian shape of the incident-beam amplitude is schematically shown. The boundary conditions along AS are: $D_0=D_h=0$. Calculations are made line by line parallel to AS. The values of D_0 and D_h at a point Q are determined from those at P and R.

perceptible effect of the boundary conditions along AS on the final solution down to the level of the integration accuracy. All the calculations were performed with data corresponding to the physical case of a 444 symmetric reflection in a silicon single crystal, with Mo $K\alpha_1$ radiation ($\theta_B=26{\cdot}9°$); for simplicity the absorption coefficient was put equal to zero.

(b) Visualization of wavefield propagation

The propagation of wavefields in the deformed crystal can be studied in the most natural way when complete maps of the field intensity in the crystal interior (*i.e.* in the Borrmann triangle) are obtained as the output of the numerical solution of Takagi's equations. The intensity at any point of the integration network is calculated as the length of the local Poynting vector:

$$\mathbf{P}=(c/\varepsilon_0)(|D_0|^2\mathbf{S}_0+|D_h|^2\mathbf{S}_h) \qquad (26)$$

and recorded line by line in the computer memory. The recordings are then transformed into intensity maps with the aid of some representation technique (lines of equal value, shades, *etc.*). In the present work the visualization procedure due to Epelboin (1978) was employed (courtesy Y. Epelboin); the maps were obtained first as images on the Tektronix TV screen and then printed on the Versatec half-tone printer. The values of intensity are represented by different grades of white, a black spot meaning very little or no intensity. As an example, a series of such maps calculated for a given value of β and three different values of η_i is shown in Fig. 6. Obviously, the principal characteristics of the beam propagation (hyperbolic trajectory) are easily recognizable on these images.

In order to extract synthetic quantitative data from our numerical calculations we developed also another technique of analyzing the beam trajectory. The method which could be simply called 'ray tracing *via* Takagi's equations' is demonstrated schematically in Fig. 7. It is based on the definition of the direction of propagation as the local direction of Poynting's vector which is given by the formula

$$\tan\varphi=\frac{1-|\xi|^2}{1+|\xi|^2}\tan\theta_B, \qquad (27)$$

φ being the angle between the direction of propagation and the reflecting planes.

An additional numerical procedure, inserted into the algorithm of integration of Takagi's equations, uses (27) explicitly to determine the local direction of propagation. It starts by calculating the initial direction $\mathbf{P}_0$ of Poynting's vector at the incidence point I_0. The value of $\xi(I_0)$ is calculated from the definition (3). At the same time the coordinates of the point Q_1 where the calculated Poynting's vector ($\mathbf{P}_0$) intersects the next line of the network are deter-

mined; the nearest point on the new line (I_1) is taken as the next point of the trajectory. There again the local value of $\xi(I_1)$ and consequently the new local direction of Poynting's vector ($\mathbf{P}_1$) are determined. This procedure is repeated iteratively as long as necessary (in the cases treated here until the crystal surface is reached). As the integration step used is very small (less than 1 μm) compared to the dimensions of the network, the whole trajectory obtained in this way is quasi-continuous.

Fig. 6(*d*) shows trajectories obtained by this method for the cases shown in Figs. 6(*a*), (*b*) and (*c*). A good correspondence with the intensity maps is easily seen. The trajectories are indeed sections of hyperbolae as predicted by the geometrical theory (§ 2) and some important parameters are more readily deducible (the coordinates x_a, z_a of the apex of the hyperbola) than from the mapping method. Besides, it is quicker and needs no visualization technique (apart from the facultative use of a plotter). Therefore, it proved to be more suitable for verification of the geometrical theory which was one of the aims of this study (§ 4). On the other hand, it is obviously less general than the method of visualization in the form of intensity maps and it fails in the case of strong deformation when the phenomenon of wavefield creation becomes important. Then trajectories obtained by this method become meaningless as the numerical procedure cannot choose between the newly created and deflected beams. In such cases (Gronkowski & Malgrange, 1984) only the direct technique of intensity mapping was applied.

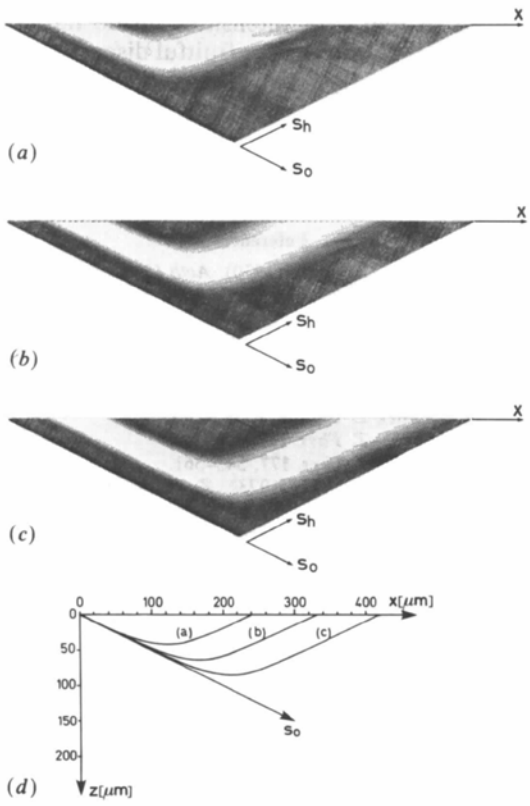

Fig. 6. Intensity distribution inside the crystal deformed with a constant strain gradient $\beta = \beta_c$ *versus* the incidence parameter η_i: (*a*) $\eta_i = -3$, (*b*) $\eta_i = -4$, (*c*) $\eta_i = -5$. The intensity maps were printed on the Versatec half-tone printer using the procedure due to Epelboin (1978) (courtesy Y. Epelboin). Here black means no intensity. (*d*) Corresponding beam trajectories obtained by the method of ray tracing *via* Takagi's equations.

4. Results and conclusions

The method of ray tracing using Takagi's equations described in § 3 was applied to verify the predictions of the geometrical theory (§ 2) for a crystal with a constant strain gradient in the symmetric Bragg case. In order to simplify the interpretation, calculations for the simple case of pure bending of lattice planes with a radius of curvature R are presented, but the same numerical results were obtained also for more complex cases (bending + lattice spacing gradient) corresponding to the same value of β.

We found that the method of ray tracing gave good results for values of $|\beta|$ not exceeding $|\beta| = 2\beta_c$, where β_c is the critical value introduced by Authier & Balibar (1970):

$$\beta_c = \pi/2\Lambda,$$

$\Lambda = \lambda \cos\theta_B / C(\chi_h \chi_{\bar{h}})^{1/2}$ being the extinction length. For such cases the intensity of the newly created wavefields was less than 5% of the incident one (see Gronkowski & Malgrange, 1984). A series of trajectories with various η_i were obtained for each of the three values of the strain gradient chosen for the calculations, *viz* $\beta = 0{\cdot}4\beta_c$, $\beta = \beta_c$ and $\beta = 2\beta_c$, respectively. Together with the complete trajectories (as those in Fig. 6*d*) the coordinates (x_a, z_a) of their apices were obtained.

The results are summarized in Fig. 8 where the values of x_e and z_a obtained using Takagi's equations (points) are compared to those (solid lines) calculated according to the geometrical theory [from (20), (18) and (19), respectively]. Very good agreement is readily seen and consequently the utility of the ray-tracing method is demonstrated.

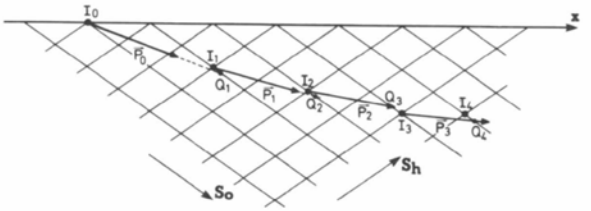

Fig. 7. Principle of the ray-tracing method. A fragment of the integration network (Fig. 5) is shown. $\mathbf{P}_i$ local Poynting vector, Q_{i+1} its intersection point with the next line, I_{i+1} the nearest point of the network which is chosen as the next point of the trajectory.

In conclusion it has to be stressed that the geometrical optics theory can be applied in all cases where beams can be defined (*i.e.* if the imaginary part of ξ is small compared to its real part) and for any strain gradient which is a smooth function of the coordinate along the reflecting planes. Although it does not take into account the phenomenon of new wavefield creation ('interbranch scattering'), its basic equations are still valid for a separate description of the trajectories of the original wavefield and the new one. This is demonstrated in the following paper (Gronkowski & Malgrange, 1984) which deals with strongly distorted crystals where the creation of new wavefields plays a significant role. It is shown in particular that this phenomenon takes place whenever the tie point of a wavefield passes through the apex of its proper branch of the dispersion surface (*i.e.* whenever $a=0$). The new wavefield extracts a fraction $\exp(-2\pi/|\alpha_0|)$ out of the original intensity, with α_0 proportional to the value of the strain gradient in the region where the creation occurs. It is then demonstrated that, provided one takes into account creation of new wavefields, geometrical optics is a quite general tool for the description of X-ray propagation in distorted crystals.

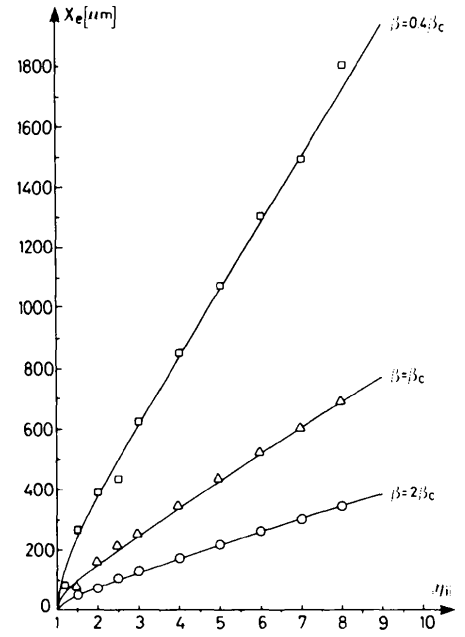

Fig. 8. Comparison between the values of $x_e(a)$ and $z_a(b)$ obtained from geometrical optics [from (20) and (19) respectively – solid lines] and those calculated from Takagi's equation (points) using the ray-tracing method described in § 3. As $\beta>0$, η_i was taken negative.

The authors wish to thank Dr Y. Epelboin for the visualization routine *PHOT5* (Epelboin, 1978) which was used to represent intensities inside the crystal and Professor A. Authier for fruitful discussions. One of us (JG) gratefully acknowledges the financial support of CNRS for a one-year stay at the Laboratoire de Minéralogie–Cristallographie.

References

AUTHIER, A. & BALIBAR, F. (1970). *Acta Cryst.* A**26**, 647–654.
AUTHIER, A. & MALGRANGE, C. (1966). *C.R. Acad. Sci.* **262**, 429–432.
AUTHIER, A., MALGRANGE, C. & TOURNARIE, M. (1968). *Acta Cryst.* A**24**, 126–136.
BEDYNSKA, T. (1973). *Phys. Status Solidi A*, **18**, 147–154.
BONSE, U. (1964*a*). *Z. Phys.* **177**, 385–423.
BONSE, U. (1964*b*). *Z. Phys.* **177**, 529–542.
BONSE, U. (1964*c*). *Z. Phys.* **177**, 543–561.
BONSE, U. & GRAEFF, W. (1973). *Z. Naturforsch. Teil A*, **28**, 558–564.
CHUKHOVSKII, F. N. (1981). *Metallofizika*, **3**, 3–30 (in Russian).
CHUKHOVSKII, F. N., GABRIELYAN, K. T. & PETRASHEN', P. V. (1978). *Acta Cryst.* A**34**, 610–621.
CHUKHOVSKII, F. N. & SHTOLBERG, A. A. (1970). *Phys. Status Solidi*, **41**, 815–825.
EPELBOIN, Y. (1978). *J. Appl. Cryst.* **11**, 676–680.
GRONKOWSKI, J. & MALGRANGE, C. (1984). *Acta Cryst.* A**40**, 515–522.
HART, M. (1980). *Elementary Dynamical Theory*, edited by B. K. TANNER & D. K. BOWEN. New York and London: Plenum Press.
KAMBE, K. (1965). *Z. Naturforsch. Teil A*, **20**, 770–786.
KAMBE, K. (1968). *Z. Naturforsch. Teil A*, **23**, 25–43.
KATO, N. (1963). *J. Phys. Soc. Jpn*, **18**, 1785–1791.
KATO, N. (1964). *J. Phys. Soc. Jpn*, **19**, 67–77, 971–985.
MALGRANGE, C. (1975). International Summer School on X-ray Dynamical Theory and Topography, Limoges, France.
PENNING, P. (1966). Thesis, Eindhoven.
PENNING, P. & POLDER, D. (1961). *Philips Res. Rep.* **16**, 419–440.
TAKAGI, S. (1969). *J. Phys. Soc. Jpn*, **26**, 1239–1253.